**DEPARTMENT OF THE ARMY**
**US ARMY RESEARCH, DEVELOPMENT AND ENGINEERING COMMAND**
**ARMY RESEARCH LABORATORY**
**ABERDEEN PROVING GROUND MD  21005-5067**

AMSRD-ARL-WM-MA

23 December 2005

MEMORANDUM FOR SEE DISTRIBUTION

SUBJECT:  ARL-TR-3241-Rev, "Hybrid Fiber Sizings for Enhanced Energy Absorption in Glass-Reinforced Composites," by Robert E. Jensen, Steven H. McKnight, Dave P. Flanagan, Alan R. Teets, and Donovan Harris

Errata sheet attached (encl) for the above-listed report.

Encl:

Robert E. Jensen, Ph.D.
Leader, Engineered Materials Team
Multifunctional Materials Branch

# ERRATA SHEET

re:  ARL-TR-3241, "Hybrid Fiber Sizings for Enhanced Energy Absorption in Glass-Reinforced Composites," by Robert E. Jensen, Steven H. McKnight, Dave P. Flanagan, Alan R. Teets, and Donovan Harris

Replace report dated July 2004 with new updated report attached (ARL-TR-3241-Rev).

ARMY RESEARCH LABORATORY

# Hybrid Fiber Sizings for Enhanced Energy Absorption in Glass-Reinforced Composites

## by Robert E. Jensen, Steven H. McKnight, Dave P. Flanagan, Alan R. Teets, and Donovan Harris

**NOTICES**

**Disclaimers**

# Army Research Laboratory

Aberdeen Proving Ground, MD 21005-5069

---

**ARL-TR-3241-Rev**                                                    **January 2006**

---

# Hybrid Fiber Sizings for Enhanced Energy Absorption in Glass-Reinforced Composites

**Robert E. Jensen, Steven H. McKnight, Dave P. Flanagan, Alan R. Teets, and Donovan Harris**
Weapons and Materials Research Directorate, ARL

# REPORT DOCUMENTATION PAGE

| 1. REPORT DATE *(DD-MM-YYYY)* | 2. REPORT TYPE | 3. DATES COVERED *(From - To)* |
|---|---|---|
| January 2006 | Final | September 1999–December 2003 |

| 4. TITLE AND SUBTITLE | 5a. CONTRACT NUMBER |
|---|---|
| Hybrid Fiber Sizings for Enhanced Energy Absorption in Glass-Reinforced Composites | |
| | 5b. GRANT NUMBER |
| | 5c. PROGRAM ELEMENT NUMBER |

| 6. AUTHOR(S) | 5d. PROJECT NUMBER |
|---|---|
| Robert E. Jensen, Steven H. McKnight, Dave P. Flanagan, Alan R. Teets, and Donovan Harris | AH42 |
| | 5e. TASK NUMBER |
| | 5f. WORK UNIT NUMBER |

| 7. PERFORMING ORGANIZATION NAME(S) AND ADDRESS(ES) | 8. PERFORMING ORGANIZATION REPORT NUMBER |
|---|---|
| U.S. Army Research Laboratory<br>ATTN: AMSRD-ARL-WM-MA<br>Aberdeen Proving Ground, MD 21005-5069 | ARL-TR-3241-Rev |

| 9. SPONSORING/MONITORING AGENCY NAME(S) AND ADDRESS(ES) | 10. SPONSOR/MONITOR'S ACRONYM(S) |
|---|---|
| | |
| | 11. SPONSOR/MONITOR'S REPORT NUMBER(S) |

**12. DISTRIBUTION/AVAILABILITY STATEMENT**

Approved for public release; distribution is unlimited.

**13. SUPPLEMENTARY NOTES**

**14. ABSTRACT**

Achieving high-impact energy absorption without loss of structural performance in a glass fiber-reinforced composite can be obtained through a "materials by design" approach of the fiber matrix interphase through modification of current commercially formulated silane-based fiber-sizing packages. In this report, we document our attempt to balance the structural and impact performance of glass-reinforced composites produced using a fiber-sizing package composed of mixed silane coupling agents to vary the reactivity of the fiber with the matrix phase. Additionally, enhancement of post-failure energy absorption through increased frictional dissipation during fiber-matrix pullout was explored through control of the surface roughness of the glass fibers. A unique inorganic-organic hybrid fiber-sizing formulation was successfully applied at a commercial E-glass manufacturing facility to produce rovings as well as woven fabric reinforcements. Composite materials were manufactured using these specialized fabrics, and the preliminary structural and impact energy responses of these materials have been measured.

**15. SUBJECT TERMS**

coupling agents, hybrid compounds, fiber/matrix bond, interphase, impact behavior

| 16. SECURITY CLASSIFICATION OF: | | | 17. LIMITATION OF ABSTRACT | 18. NUMBER OF PAGES | 19a. NAME OF RESPONSIBLE PERSON<br>Robert E. Jensen |
|---|---|---|---|---|---|
| a. REPORT | b. ABSTRACT | c. THIS PAGE | UL | 36 | 19b. TELEPHONE NUMBER *(Include area code)* |
| UNCLASSIFIED | UNCLASSIFIED | UNCLASSIFIED | | | 410-306-1910 |

# Contents

## List of Figures

## List of Tables

# Acknowledgments

# 1. Introduction

While the quasistatic mechanical performance benefits of fiber-reinforced composites are often the reason for their selection in structural applications, it is generally accepted that the response of the fiber-matrix interphase region can contribute to impact resistance and damage tolerance (1–3). The effect of the interphase on impact performance is largely determined by the choice of sizing components applied during glass fiber production (4–7). Previously published results indicate that the impact response of a fiber-reinforced composite can be tailored towards high energy absorption by engineering weak fiber-matrix interfacial interactions; or, conversely, high damage tolerance (e.g., residual strength after impact) can be produced by promoting strong fiber-matrix interfacial interactions (8). Impact-damaged composite panels that are constructed using glass fibers that adhere poorly to the polymer matrix display large damage areas due to extensive fiber-matrix debonding, pullout, and delamination mechanisms. These micromechanical processes result in high energy absorption during impact. As the fiber-matrix bond strength is increased, energy absorption during impact decreases. Significant fiber breakage during impact dominates the failure and less fiber-matrix debonding and pullout are observed.

The interphase response can be controlled by appropriate selection of sizing components. Silane coupling agents are important constituents in the multicomponent fiber-sizing formulations applied to the fibers during production (9–11). The effect of silane coupling agents and silane-based sizings on glass fiber-reinforced composite structural performance and durability has been widely studied (12–17). Traditionally, silane coupling agents are used to increase the adhesion of the glass fiber reinforcement to the polymeric matrix and to increase the strength retention of the composite upon exposure to wet conditions (18, 19). Common silane coupling agents used to increase the structural performance/moisture resistance of glass-reinforced composites incorporate epoxy, amine, or methacryl functional groups as the reactive organic component, depending on the chemistry of the matrix resin (20, 21). The silane coupling agent comprises ~10 weight percent of the total solids present in a typical formulation. The role of the silane and the other constituents, including film formers, surfactants, and lubricants, found in more complex commercial sizings has been investigated more thoroughly in other research (22).

Recent studies have started to quantify the energy absorption mechanisms of the fiber-matrix interphase during high strain rate single fiber push-out experiments (23, 24). These studies propose two distinct regions of energy absorption attributed to fiber-matrix debonding and post-debonding frictional sliding. In general, the systems studied showed strong rate dependence before, during, and after fiber-matrix debonding; and the post-debonding frictional sliding mechanism was found to absorb the greatest amount of energy. These studies lead to the two following questions: Is it possible to control the strength of the fiber-matrix interphase as a

function of loading rate through careful design and selection of sizing components? Is it possible to increase the energy absorption during post-debonding frictional sliding? These questions provided the motivation for development of a new class of fiber sizings and the following paragraphs describe the reasoning that was followed for the formulation development.

Traditional approaches to sizing fiber for either structural or impact performance in a composite material would dictate that either the fiber be made as chemically reactive as possible or as inert as possible, respectively, towards the polymeric matrix. A logical approach to obtain intermediate structural and impact performance would be to impart intermediate levels of adhesion between the fiber and matrix. Published studies have been conducted where the density of reactive "sticker" groups along the main backbone chains and corresponding density of reactive "receptor" groups found on the surface of the substrate have been varied and the adhesion strength measured (25). In this research, the maximum adhesive strength was achieved through a relatively low number of receptor-sticker group interactions indicating full reactivity is not necessary for maximum adhesion. Similar research on the adhesion of thermosetting epoxy adhesives to silicon wafers treated with varying degrees of octadecyltrichlorosilane, which interacts weakly with the epoxy adhesive (26). This study yielded a comparable result in that the epoxy adhesive required a relatively low density of strong surface interactions with the substrate to exhibit maximum bond strength. More importantly, the concentration of sticker groups at which maximum adhesion was observed was found to be temperature dependent, with larger numbers of strong interactions required to maintain high bond strength as the temperature was decreased. Time-temperature equivalence of polymeric materials suggests that this adhesion behavior may also be rate dependent. In other words, a careful adjustment of the fiber-matrix reactivity through formulation of matrix-compatible and matrix-incompatible silane coupling agents could potentially yield strong fiber-matrix interactions at low strain rates and weak fiber-matrix interactions at high strain rates.

After fiber-matrix debonding has occurred, it would be desirable to maximize post-failure frictional energy absorption mechanisms via fiber pullout. Microscale interface testing using a microdrop pull-off method has shown the impact of nano-textured fiber surfaces on energy absorption in model systems (27). Fiber surfaces were textured using a sol-gel synthesis of multiple alkoxy silanes. Using blends of tri-alkoxy silane coupling agents employed in traditional sizing systems and tetraethoxysilane (TEOS), a variety of textured surfaces were created on glass fiber surfaces. The resulting texture was influenced through control of the reaction conditions, acidic or basic catalyst concentrations, and inorganic-organic stoichiometry ratios. The alkoxy sol-gel chemistry was an attractive approach to modifying fibers surfaces guided by the established literature on sol-gel coatings (e.g., formulations to increase the scratch resistance of glass) (28–31). Other researchers have used colloidal silica to enhance the adhesion of glass fibers to polypropylene via dip-coating methodologies (32). This is potentially a simpler technique than sol-gel chemistry to increase the surface roughness of commercially produced

glass fibers, thereby increasing the coefficient of friction between the fiber and matrix during the fiber pullout stages of composite failure. To our knowledge, the use of preformed colloidal silica particles has yet to be applied to commercial glass fiber sizings.

If the previous arguments pertaining to the energy absorption mechanisms due to fiber-matrix bond strength and fiber-surface roughness carry some validity, then the ideal fiber sizing for both optimal structural and impact performance should, in theory, be composed of a mixture of silane coupling agents to vary the fiber reactivity towards the matrix phase and some type of hard inorganic phase to increase the roughness of the fibers. The relationship between the fiber surface reactivity and surface roughness would also certainly be coupled with each other. If there is too little chemical reactivity between the fiber and matrix, then the transfer of stress is inefficient and the composite will show poor structural response. If the chemical reactivity between the fiber and matrix is too strong, then stress transfer between the fiber and matrix results in fiber breakage, which negates the effects of increased surface roughness and energy dissipation through frictional sliding. In this report, we document our attempt to balance the structural and impact performance of glass-reinforced composites produced using a fiber-sizing package composed of mixed silane coupling agents to vary the reactivity of the fiber with the matrix phase. Additionally, enhancement of post-failure energy absorption through increased frictional dissipation during fiber-matrix pullout was explored through control of the surface roughness of the glass fibers. A unique inorganic-organic hybrid fiber-sizing formulation was successfully applied at a commercial E-glass manufacturing facility to produce rovings as well as woven fabric reinforcements. Composite materials were manufactured using these specialized fabrics and the preliminary structural and impact energy responses of these materials have been measured.

## 2. Experimental

### 2.1 Fiber-Sizing Packages

A series of sizing packages were evaluated in this study using commercially available materials generally used by the glass fiber industry (*33*). In this work, the epoxy-incompatible and epoxy-compatible silane coupling agents were n-propyltrimethoxysilane (PTMO) and 3-glycidoxypropyltrimethoxysilane (GPS), respectively. In cases where increased fiber surface roughness was desired, colloidal silica with an average particle diameter of 22 nm was added to the fiber-sizing package. In all cases, a water-dispersible diglycidyl ether of bisphenol A epoxy (DGEBA) was implemented as the film former. Four specific sizings are reported here: (1) a "hybrid" fiber-sizing package consisting of a mixture of GPS, PTMO, and the colloidal silica fiber surface roughening agent; (2) an "incompatible" fiber-sizing package containing only PTMO, which has no chemical reactivity towards an epoxy-based matrix; (3) a "compatible" fiber-sizing package containing only GPS, which is highly chemically reactive towards an

epoxy-based matrix; and (4) a "mixed" fiber-sizing package consisting of the identical ratio of GPS to PTMO coupling agents as found in the "hybrid" fiber-sizing package, but without the colloidal fiber-surface roughening agent. These sizing materials are summarized in table 1. The aqueous-based fiber-sizing packages were formulated within concentration ranges conducive for industrial production, generally 5–10% solids in water, including film formers and surfactants. Successful pilot plant scale-up of selected sizing formulations was completed by Fiber Glass Industries, Inc. (FGI), Amsterdam, NY. The laboratory sizing formulations were modified slightly by FGI to incorporate minor amounts of additional proprietary lubricants, antistatic electricity agents, and other processing aids. Single-end E-glass rovings were manufactured with a 454-kg/m (225-yd/lb) yield, M filaments (~16-μm diameter), and a roving count of 4000 filaments. The custom-sized rovings were subsequently woven into 0.81 kg/m$^2$ (24 oz/yd$^2$) plain weave fabrics.

Table 1. Summary of materials used in fiber-sizing compositions. 3-glycidoxypropyltrimethoxy silane (GPS) was used as the reactive-compatible coupling agents and n-propyltrimethoxysilane (PTMO) was the nonreactive-incompatible silane coupling agent. Colloidal silica was used as the roughening agent.

| Fiber Sizing | Silanes | Film Former | Roughening Agent |
|---|---|---|---|
| Hybrid | GPS PTMO | DGEBA epoxy dispersion | Water dispersible colloidal silica |
| Compatible | GPS | DGEBA epoxy dispersion | None |
| Mixed | GPS PTMO | DGEBA epoxy dispersion | None |
| Incompatible | PTMO | DGEBA epoxy dispersion | None |

## 2.2   Roving Strength

Increased fiber-fiber and tow-tow friction during the initial fiber processing stages at the glass manufacturing and weaving facilities is undesirable, as increased friction leads to fiber breakage and processing difficulties. To verify that the film former, lubricants, and other processing aids of the fiber-sizing package remain effective upon incorporation of the inorganic fiber surface roughening agent, the fiber roving strengths were measured both before and after weaving using a modified version of ASTM D 3379-75 (*34*). The methodology was modified to measure the tensile strengths of an entire bundle of roving filaments, rather than single filaments as specified. This procedural modification was made to simplify the experiments, as the results were intended to be comparative. Tensile force (*P*) measurements were measured using a crosshead rate of 1.27 mm/min with a sample gauge length of ~152 mm. Tensile strengths (*T*) were calculated using the following expression:

$$T = \frac{P}{A},$$ (1)

where *A* represents the calculated cross-sectional area of the roving based on the roving bundle count of 4000 filaments and filament diameter of 16 μm. Tensile strengths were measured for fiber bundles treated with the hybrid sizing and compatible sizing taken from spools before

fabric weaving and from woven fabric for comparison.  The roving strength measurements were taken as an estimate of the processing characteristics of the hybrid fiber-sizing package with direct comparisons to the industrial-standard compatible fiber-sizing package.  The reported values represent an average of the five samples tested for each roving type.

## 2.3   Pultruded Rod Composite Fabrication

Prior to receiving woven fabrics, spools of individual roving packages treated with the hybrid and compatible sizing formulations were received from FGI.  The roving packages were used to produce unidirectional, fiber-reinforced pultruded composite rods using the methods outlined by Thomason (*35*) and Gorowara (*36*).  The composite rods were prepared with a volume fraction of fiber equal to ~0.50.  The matrix resin consisted of Applied Poleramic, Inc., SC15, a two-part, low-viscosity toughened epoxy resin with amine curing agents.  After mixing the resin and curing agent according to manufacturer's specifications, the mixed resin was de-gassed under vacuum at 50 °C until no air bubbles were present.  The resin was then poured over the fiber rovings and infused using a hand roller and the wet fiber rovings were pulled through a fluoropolymer tube with an inside diameter of 9.53 mm.  The fluoropolymer tube was then inserted into a close-fitting copper pipe for support to ensure alignment of the cured composite rods.  The composite rods were cured at 200 °C for 3 hr under slight tension with the use of a hanging weight.  To minimize thermal stresses, the composite samples were slowly cooled in the oven until they equilibrated at room temperature.

## 2.4   Composite Panel Fabrication

Composite panels with approximate dimensions of $500 \times 500 \times 6.35$ mm were fabricated using a vacuum-assisted resin transfer molding (VARTM) process (*37*).  The woven fabric was stacked using 0°–90° fabric lay-ups.  The SC15 epoxy resin was used following the same mix ratios and cure schedule as the composite rods.  Fiber volume fractions of the cured composite panels were calculated using rules of mixtures and experimentally measured values of density.  The density measurements were undertaken using the ASTM D 792-00 testing standard and minimums of five samples for each data set (*38*).  Final volume fractions of glass fiber present in the composite panels were calculated to lie between 0.55 and 0.56 for all samples tested.  Void contents of the cured composite panels were not determined, however void contents of <2% are typical.

## 2.5   Short Beam Shear Testing

The composite rods were sectioned into lengths of 60 mm, and the apparent short beam shear strength was measured using ASTM D 4475-85 (*39*) using a 3-point bending apparatus.  The testing standard allows for the span (*s*) to diameter (*d*) ratio to vary from 3:1 to 6:1, with an *s:d* ratio of 5:1 reported in this research.  For each fiber-sizing condition, a minimum of five samples were tested using an Instron model 4505 equipped with an 89-kN load cell at a crosshead rate of 1.27 mm/min.  The interfacial shear strength (IFSS) was calculated using the following equation, where *P* is the measure force at failure:

$$IFSS = \frac{0.849P}{d^2}.\tag{2}$$

Composite rods were tested immediately following initial processing and after submersion in water at 70 °C for 30 days.

## 2.6 Flexural Strength

Flexural strength was measured with 127- × 25.4- × 6.35-mm composite panel samples using the ASTM D 790-96a testing method (*40*). The test was carried out in the 3-point bending mode configuration. Testing was completed with the span length (*L*) to width (*b*) ratio set to the standard 16:1 using a minimum of five samples for each fiber-sizing condition. An Instron model 4505 equipped with an 89-kN load cell was used at a crosshead rate of 1.27 mm/min. Breaking force (*P*) was taken from force-vs.-displacement data and the maximum fiber stress ($\sigma_{max}$) was calculated using the following equation:

$$\sigma_{max} = \frac{3PL}{2bd^2},\tag{3}$$

where *d* represents the sample thickness.

## 2.7 Tensile Strength

The tensile properties of the composite samples were determined according to the ASTM D 3039 testing method (*41*). An Instron model 1125 equipped with an 89-kN load cell was used at a crosshead rate of 2.54 mm/min, and at least three samples were tested for the compatible and hybrid fiber-sizing conditions. Average sample dimensions were 152 × 25.4 × 3.5 mm. Breaking forces (*P*) were taken from force-vs.-displacement plots and the ultimate tensile strength ($F^{tu}$) was calculated using the following equation:

$$F^{tu} = \frac{P}{bd}.\tag{4}$$

## 2.8 Drop Tower Impact Testing

The impact properties of the composite panels were measured using a Dynatup Drop Weight System. Samples were cut into 100- × 100- × 6.35-mm squares and impacted with a 12.7-mm-diameter hemispherical impact striker. Plots of the impact force ($P_{impact}$) vs. time are shown in the results section. Experimentally measured values of impact energy ($E_{impact}$), impact velocity ($V_{impact}$), and maximum force ($P_{max}$) were recorded from the instrument and are also summarized in the results section. The impact energy absorbed to maximum force ($E_{max}$) and total energy absorbed ($E_{total}$) were calculated using the instrument software (*42*). Deflection data was not recorded.

To measure the projected post-impact damage area the damage zone was first visually observed using a light box and outlined with a black permanent marker pen.  A digital image was then taken of each damaged panel and a pixel area ratio of the projected damaged area to undamaged area was analyzed using an image analysis software package (*43*).  Actual projected damage area could then be determined by simply multiplying the actual sample dimensions by the computer generated pixel ratio.  Composite panels were impact tested immediately following initial processing and after submersion in water at 70 °C for 30 days.  Minimums of four samples were tested for each composite panel set.  Smaller 12- × 12- × 6.35-mm sections of composite panel were also subjected to moisture exposure at 70 °C for 6 months to monitor uptake mass.

## 2.9   Compression After Impact Strength

The compression after impact (CAI) properties of the composite panels were measured using the SACMA recommended method SRM 2R-94 (*44*).  Impact damage was generated using the Dynatup Drop Weight System.  Samples were cut into 150- × 100- × 6.35-mm rectangles and impacted with a 15.9-mm diameter hemispherical impact striker.  The mass and drop height of the impacter were adjusted to provide an impact energy of 42.6 J, which closely approximates the energy level of 6.7 J/mm of composite thickness as specified in the standard.  Once damaged, the residual compressive strengths of the samples were measured using an Instron model 1332 servo-hydraulic machine equipped with a 222.4 kN load cell.  A Boeing CAI loading test fixture (Wyoming Test Fixtures, Inc.) was used at a crosshead rate of 2.54 mm/min.  Ultimate Compressive strength ($\sigma_{ult}$) was calculated using the following expression:

$$\sigma_{ult} = \frac{P}{bd}.$$  (5)

Minimums of five samples were tested for each fiber-sizing condition.

# 3.   Results and Discussion

## 3.1   Fiber and Roving Characterization

The primary roles of the film former and lubricant constituents of a commercial fiber-sizing package are to reduce the processing friction experienced by the fiber rovings during fabric weaving.  Lowered levels of processing friction result in decreased fiber breakage, hence retention of high tensile strength in the final composite assembly.  During resin infusion and subsequent cure of the composite assembly, the film former and lubricants diffuse from the surface of the fibers into the matrix resin, which exposes the silane coupling agent network on the fiber surfaces (*36*).  In the case of the hybrid fiber-sizing package, the fiber surfaces are intentionally roughened to promote increased friction during fiber-matrix pullout in fully cured composite assemblies.  However, the effects of the inorganic fiber surface roughening agent are not desirable during roving manufacturing processes, such as weaving.

Figure 1 shows a scanning electron microscopy (SEM) image of a compatible-sized fiber, after solvent rinsing the soluble portions of the sizing package. This SEM image reveals a mostly smooth fiber surface morphology, with the exception of a few defect sites in the glass, as expected. Upon addition of the inorganic surface-modifying agent to the hybrid fiber-sizing package, the surface morphology of the glass fiber changes dramatically, as seen in figure 2. The fiber surfaces displayed in figures 1 and 2 represent the "idealized" regions envisioned during conceptualization and development of the hybrid fiber-sizing package. Low magnification SEM images of the hybrid sized fiber samples, which are not shown, displayed a higher degree of heterogeneous deposition of the inorganic fiber surface-modifying agent onto the surfaces of the fibers. Thus, it would be expected that a more in-depth atomic force microscopy (AFM) analysis would also yield varying measures of surface roughness. In addition, SEM characterization of hybrid fiber sizing provides no indication of covalent bonding of inorganic surface modifying agent to glass fiber surface, although the fibers were rinsed in solvent. Some percentage of the inorganic fiber surface-modifying agent present in the hybrid fiber-sizing package may have been washed from the fiber surfaces during the solvent rinse.



Figure 1.  SEM image of E-glass fiber surface treated with compatible
sizing after acetone rinse to extract soluble fractions of film
former, surfactant, lubricants, and other processing additives.

To ensure that the film former and lubricants of the hybrid fiber-sizing package adequately protect the fibers during processing, the tensile strengths of roving bundles were measured. The average tensile strengths of the hybrid and compatible-sized fiber roving bundles were 0.97 $\pm$ 0.09 GPa and 1.17 $\pm$ 0.09 GPa, respectively. Brown et al. reported a very similar experimental methodology for the determination of E-glass fiber bundle strengths, but applied a more rigorous Weibull analysis in the calculations (*45*). These researchers determined average tensile strengths
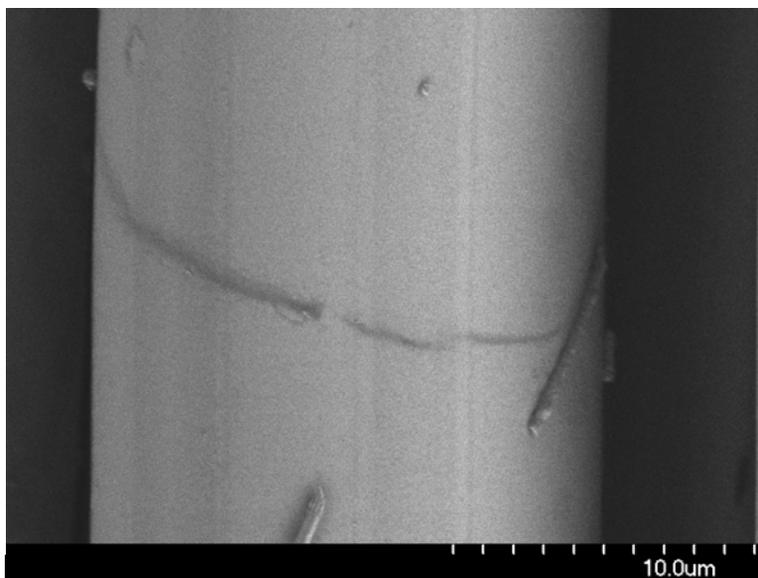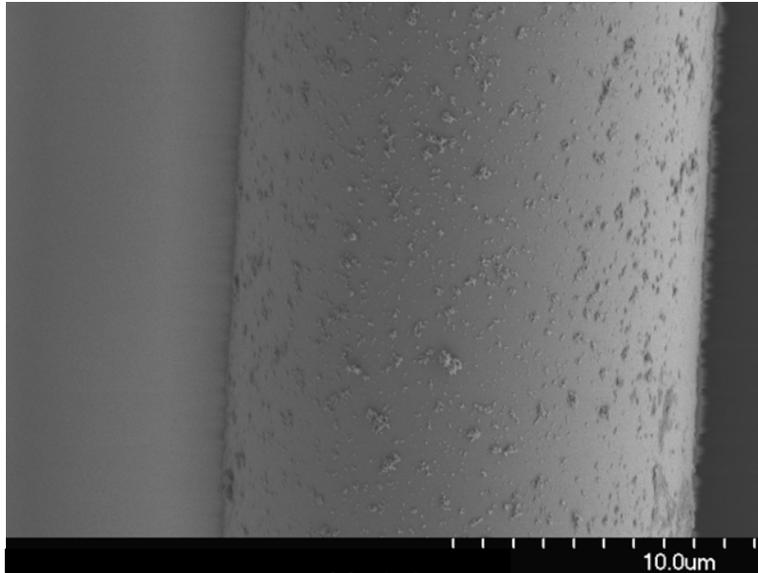
Figure 2.  SEM image of E-glass fiber surface treated with hybrid
          sizing after acetone rinse to extract soluble fractions of film
          former, surfactant, lubricants, and other processing additives.

of ~1.3 to 1.9 GPa, based upon an average filament diameter of 9 µm and 204 filaments per bundle.  Therefore, it appears that the roving bundle tensile strengths reported for this research are reasonable, considering that a 16-µm filament used for this research should have a lower tensile strength than the 9-µm filament reported in the literature (*46*).  These results indicate that the inorganic surface-modifying agent of the hybrid fiber-sizing package appears to cause minimal additional fiber breakage during commercial manufacturing and should be cause for minimal concern when considering fiber-processing characteristics.

Production of commercial woven roving fabric for composite panel fabrication is a large-scale and costly operation with up to hundreds of individual spools of roving packages required to weave as little as 100 m of usable fabric.  Therefore, to minimize the risk associated in transitioning the ARL-derived experimental fiber-sizing package from the bench-top to application at FGI's production facility, a limited number of individual roving packages were produced to gauge the feasibility of successful larger-scale production runs.  Chronologically, these roving packages were first used for the fiber characterization and tensile strength measurements previously described.  Furthermore, the individual roving packages were also used to generate preliminary composite mechanical property measurements to provide confidence in the production of the multitude of roving packages required to set-up a large commercial loom for weaving into fabric.  Composite fabrication options are limited with individual spools of glass fiber roving, with a cylindrical composite rod being one of the simplest configurations to fabricate at a laboratory scale.

The mechanical properties of the epoxy matrix/glass fiber-reinforced composite rods with hybrid-sized fibers were directly compared to those reinforced with the standard matrix compatible-sized fibers. The IFSS values of the cylindrical composite rods with glass reinforcement treated with the hybrid and compatible sizings were 41.7 ± 2.7 MPa vs. 39.8 ± 4.7 MPa, respectively. The samples failed in interlaminar shear regardless of fiber sizing that was used. The quasistatic IFSS response of the composite rods reinforced with either the hybrid- or compatible-sized fibers were approximately equivalent, which was one of the goals outlined when formulating the ARL hybrid fiber sizing. The results obtained from the initial fiber surface SEM characterization, roving tensile measurements, and IFSS measurements of the epoxy matrix based composite rods provided the confidence to scale-up for the much larger amount of material needed for weaving.

## 3.2  Composite Tensile and Flexural Properties

Flat epoxy matrix-based composite panels were fabricated using the 0.81 kg/m$^2$ (24 oz/yd$^2$) plain weave fabric subsequently produced by FGI. The flat composite panels measured ~6.35 mm in thickness and were processed using the VARTM procedure outlined in the experimental section. While woven fabric was obtained with the hybrid, incompatible, compatible, and mixed fiber sizings, only the mechanical properties of the hybrid sizing and epoxy compatible sizing are reported. The ultimate tensile strengths ($F^{tu}$) measured for the composite samples increased slightly for the hybrid fiber sizing in comparison to the compatible fiber sizing, 368 ± 14 MPa vs. 348 ± 16 MPa, respectively, with the tensile failure modes of both samples appearing identical. As the roving tensile strengths of the hybrid and compatible-sized fibers are very similar, it is not surprising that the tensile strengths of the respective composite samples were very close in magnitude. The average maximum fiber flexural stress ($\sigma_{max}$), or flexural strength, was lower for the hybrid fiber-sized composites when compared to the compatible fiber-sized composites, 411 ± 16 MPa vs. 506 ± 17 MPa, respectively. Both samples failed primarily in a tension mode in the center of the sample coupons, however, the composite samples reinforced with the hybrid-sized fibers appeared to have slightly more compressive damage at the center loading point of the 3-point bend test fixture. This possible additional compression damage could be related to the lower flexural strength. While more detailed mechanical analysis are planned for future work, the preliminary mechanical testing results seem to indicate that the hybrid fiber-sizing formulation could have the potential to closely match the mechanical properties offered by traditional matrix compatible fiber sizings.

## 3.3  Composite Impact Properties

Low-velocity, drop-tower impact testing of composite panels can be performed with relative ease, however the role of test set-up, sample constitutive properties, interpretation of the damage modes, and quantification of the resultant data is often complex. The kinetic energy and velocity of the drop tower impact striker, which are governed through Newton's second law of motion, can be adjusted via drop height and/or drop mass. For this comparative study, three different

impact energies were tested, referred to as low ($E_{impact}$ = 37 J), medium ($E_{impact}$ = 80 J), and high ($E_{impact}$ = 124 J). The impact energy was adjusted by adding drop mass to the impact striker frame while the drop height remained constant, thus the impact velocity also remained constant. The converse scenario of altering drop heights, hence impact velocities, was not investigated for this study. Additionally, a wide variety of impact striker geometries are available, which could bias differing stress states during the impact loading and cause varying response mechanisms in the composite. Therefore, the impact striker tip geometry was also kept constant during this study.

Although the fiber-matrix interphase was the focus of this study, there are numerous other constitutive materials properties of the composite that dictate impact response, such as fiber strength, matrix toughness, matrix stiffness, fabric structure, fabric cross-ply orientation, fiber-volume fraction, and boundary conditions (*47–50*). Impact energy-absorbing mechanisms include matrix cracking, fiber fracture, delamination, debonding, and fiber pullout (*8*). Rigorous analysis and interpretation of the impact response and damage modes in composite materials have been derived using inelastic energy curves, which couple the returned energy and incident-impact energy (*51, 52*). Other researchers have proposed progressive impact fracture models to predict the energy absorption properties of composite materials (*53*). The objective of this current research was to solely examine the effects of the fiber sizing to the impact response of the composite, thus all other sample parameters were kept constant and comparative analysis was limited to interpretation of impact force-vs.-time curves, measured energy-absorption values, and visual inspection of the damaged samples.

The representative force-vs.-time curves for the composite panels reinforced with compatible-sized fibers during impact testing are shown in figure 3. Minimal fiber breakage was observed at the low- and medium-impact energies. However, at the high-impact energy, significant fiber breakage and push-out through the back sides of the sample plates occurred, which resulted in a sharp drop in the force response immediately following the force-vs.-time peak maximum. This type of response was expected due to the presumably high levels of adhesion between the compatible-sized fibers and matrix, which allows maximum stress transfer from the matrix to the fibers. Quantitatively, the high degree of stress transfer to the fibers allows for a relatively high level of $P_{max}$ sustained during the impact event (18.8 ± 1.6 kN), prior to fiber failure. However, the subsequent high degree of fiber breakage and push-out leads to low values of $E_{max}$ (80.4 ± 12.7 J) and high values of $E_{total}$ (123.6 ± 3.1 J), as summarized in table 2. Simply stated, impact striker of the drop tower test fixture strikes the compatible-sized fiber-reinforced composite samples and pushes out the back side of the plate with no impact striker rebound.

The force-vs.-time curves for the composite panels reinforced with incompatible-sized fibers during impact testing are shown in figure 4. The impact performance of this sample at low- and medium-impact energies resulted in larger overall damage areas when judged against the

Figure 3.  Representative force-vs.-time curves for flat E-glass composite
panel treated with compatible sizing during impact testing.
(▼) $E_{impact}$ = 37 J, (■) $E_{impact}$ = 80 J, (▲) $E_{impact}$ = 124 J,
$V_{impact}$ = 4.5 m/s.

Table 2.  Summary of drop-tower impact testing results for composite panels with E-glass fibers treated with
hybrid, compatible, mixed, and incompatible fiber sizings.  Error represents one standard deviation.

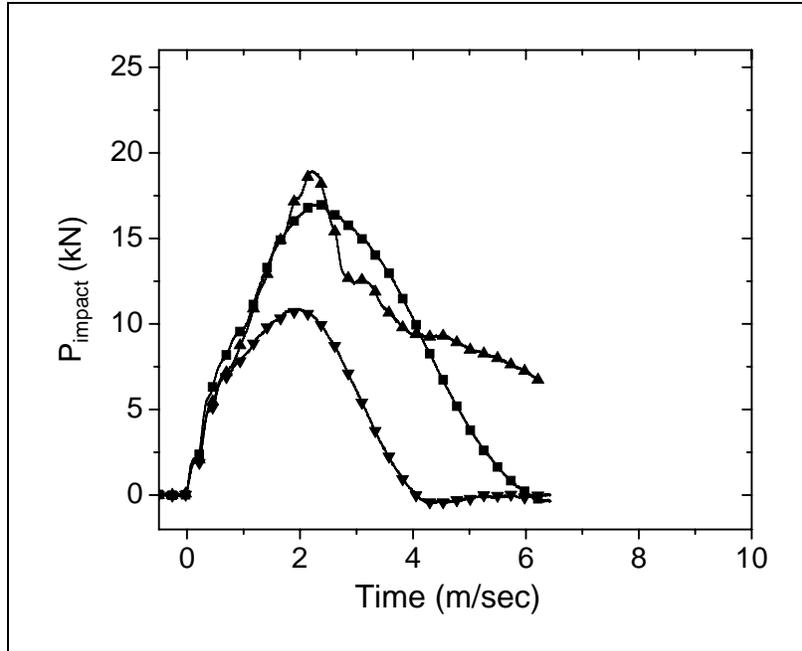| Fiber Sizing | $E_{impact}$ (J) | $P_{max}$ (kN) | $E_{max}$ (J) | $E_{total}$ (J) | Damage Area (mm²) |
|---|---|---|---|---|---|
| Hybrid | 37.1 ± 0.1 | 11.0 ± 0.1 | 36.6 ± 0.2 | 23.0 ± 0.1 | 680 ± 20 |
| Compatible | 37.0 ± 0.1 | 10.9 ± 0.2 | 36.6 ± 0.1 | 23.4 ± 0.5 | 670 ± 110 |
| Mixed | 37.0 ± 0.1 | 11.8 ± 0.1 | 36.8 ± 0.1 | 19.2 ± 0.1 | 590 ± 40 |
| Incompatible | 37.1 ± 0.1 | 11.0 ± 0.1 | 36.6 ± 0.2 | 20.5 ± 0.4 | 1290 ± 370 |
| | | | | | |
| Hybrid | 80.5 ± 0.3 | 18.1 ± 0.1 | 78.8 ± 2.3 | 45.1 ± 1.0 | 2020 ± 240 |
| Compatible | 80.5 ± 0.3 | 17.3 ± 0.3 | 73.2 ± 4.9 | 51.2 ± 1.4 | 960 ± 70 |
| Mixed | 80.9 ± 0.4 | 18.6 ± 0.1 | 77.5 ± 4.3 | 45.9 ± 2.5 | 900 ± 50 |
| Incompatible | 81.0 ± 0.2 | 16.1 ± 0.2 | 77.3 ± 1.0 | 52.2 ± 0.1 | 3350 ± 500 |
| | | | | | |
| Hybrid | 123.7 ± 1.0 | 20.9 ± 0.8 | 110.5 ± 7.8 | 89.6 ± 4.1 | 2610 ± 210 |
| Compatible | 124.2 ± 1.3 | 18.8 ± 1.6 | 80.4 ± 12.7 | 123.6 ± 3.1 | 1300 ± 120 |
| Mixed | 125.8 ± 0.4 | 19.7 ± 0.9 | 87.7 ± 9.8 | 105.1 ± 2.6 | 1330 ± 170 |
| Incompatible | 125.8 ± 0.3 | 17.8 ± 0.4 | 102.4 ± 9.6 | 98.9 ± 2.5 | 4400 ± 190 |
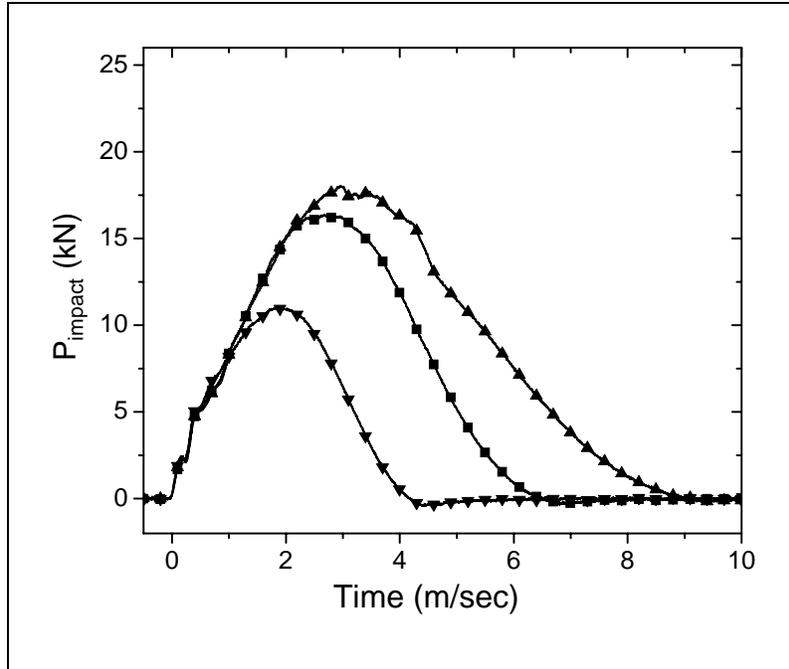
Figure 4. Representative force-vs.-time curves for flat E-glass composite
panel treated with incompatible sizing during impact testing.
($\blacktriangledown$) $E_{impact}$ = 37 J, ($\blacksquare$) $E_{impact}$ = 80 J, ($\blacktriangle$) $E_{impact}$ = 124 J,
$V_{impact}$ = 4.5 m/s.

composite panels reinforced with compatible-sized fibers, as summarized in table 2. However,
the impact response of the incompatible sizing was remarkably different at high-impact energies,
with a gradual rolling over of the force-vs.-time curve. The presumably low levels of adhesion
between the incompatible-sized fibers and epoxy matrix allow the fibers to debond at the fiber-
matrix interphase and slide through the matrix, rather than breaking. This fiber-matrix
debonding mechanism yields a low degree of stress transfer from the matrix to the fibers, which
resulted in the lowest observed levels of $P_{max}$ sustained during the high-energy impact events
(17.8 ± 0.4 kN). The composites panels reinforced with incompatible-sized fibers displayed
significantly larger damage areas than the composite panels reinforced with compatible-sized
fibers at the high-impact energy level, but no significant fiber breakage or push-out through the
back sides of the samples were observed. In comparison to the compatible fiber-sizing
treatment, the incompatible fiber-sizing treatment results in greater values of $E_{max}$ (102.4 ± 9.6 J)
and lower values of $E_{total}$ (98.9 ± 2.5 J). The lower value of $E_{total}$ (<124 J) was evident during the
impact testing as the impact striker of the drop tower fixture rebounded upward from the
composite plate after the initial strike.

The representative force-vs.-time curves for the composite panels reinforced with mixed-sized
fibers during impact testing are shown in figure 5. These results were interesting in that the
impact-response curves appear to be very similar to those of the compatible fiber sizing at the
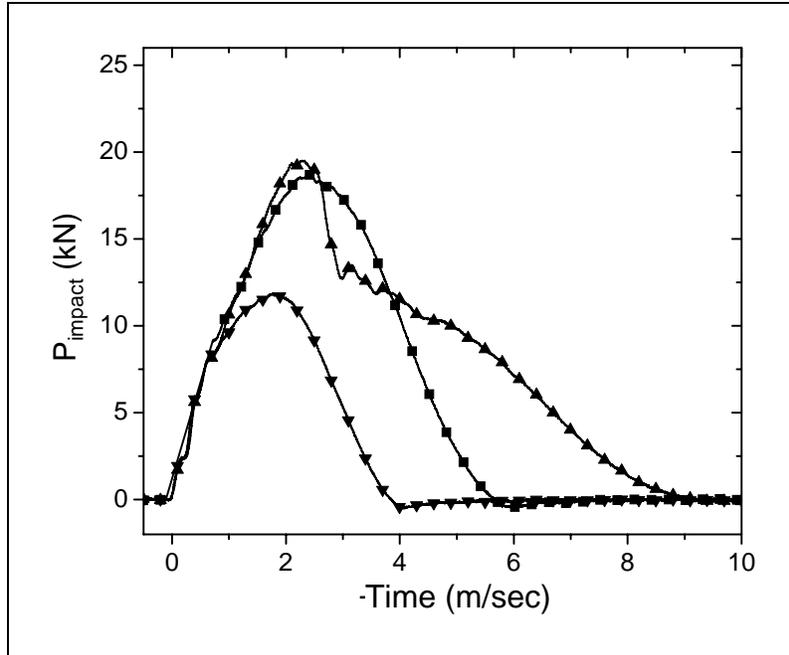
Figure 5. Representative force-vs.-time curves for flat E-glass composite
panel treated with mixed sizing during impact testing.
($\blacktriangledown$) $E_{impact}$ = 37 J, ($\blacksquare$) $E_{impact}$ = 80 J, ($\blacktriangle$) $E_{impact}$ = 124 J,
$V_{impact}$ = 4.5 m/s.

low- and medium-impact energies. The overall damage areas and visually observed levels of
fiber breakage and push-out remained close to those values determined for the composite panels
reinforced with the compatible-sized fibers, as summarized in table 2. The similarity in damage
mechanisms to the composite samples reinforced with the compatible-sized fibers is reflected in
comparable $P_{max}$ average values sustained during the high-energy impact events (19.7 ± 0.9 kN).
However, the energy absorption values for this sample reflect coupled behavior between the
compatible and incompatible fiber sizings with intermediate values of $E_{max}$ (87.7 ± 9.8 J) and
$E_{total}$ (105.1 ± 2.6 J).

The characteristic force-vs.-time curves for the composite panels reinforced with hybrid-sized
fibers during impact testing are shown in figure 6. The impact-response curves were very similar
in appearance to those of the incompatible fiber sizing. However, $P_{max}$ achieved during the high-
energy impact was greater for the hybrid sizing than the incompatible sizing, 20.9 ± 0.8 kN vs.
17.8 ± 0.4 kN, respectively. The damage areas measured for the hybrid-sized fiber-reinforced
composites were also interesting. At low-impact energies, the total damage area of the hybrid
sizing was equivalent to those of the compatible- and mixed-fiber sizings. As the impact energy
was increased, the damage area became larger in comparison to the compatible- and mixed-fiber
sizings, but always remained less than the damage areas of the incompatible fiber sizing. At the
high-impact energy, the hybrid fiber sizing experienced minimal fiber breakage and no fiber
push-out due to the drop tower impact striker. In comparison to the compatible, incompatible,
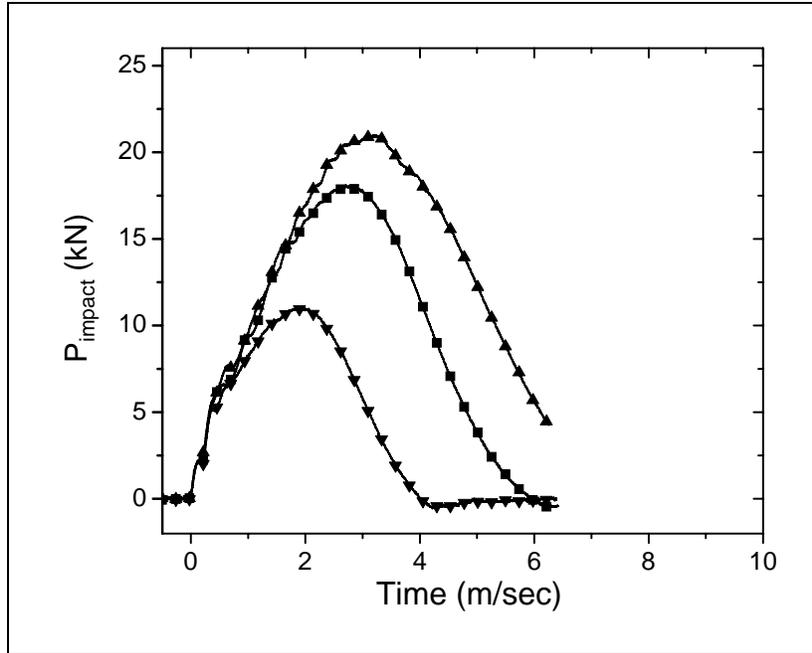
14

Figure 6.  Representative force-vs.-time curves for flat E-glass composite
panel treated with hybrid sizing during impact testing.  ($\blacktriangledown$) $E_{impact}$
= 37 J, ($\blacksquare$) $E_{impact}$ = 80 J, ($\blacktriangle$) $E_{impact}$ = 124 J, $V_{impact}$ = 4.5 m/s.

and mixed fiber-sizing treatments, the hybrid fiber-sizing treatment resulted in greatest average value of $E_{max}$ (110.5 ± 7.8 J) and lowest average value of $E_{total}$ (89.6 ± 4.1 J).  The hybrid fiber sizing outperformed the incompatible sizing in terms of $E_{max}$, which is indicative of excellent impact properties, and outperformed the compatible and mixed fiber sizings in terms of $P_{max}$, which is indicative of excellent structural response.  The preliminary impact testing performed for this research shows that the hybrid fiber sizing has potential to fulfill the role of a simultaneous impact and structural sizing.  An overlay of the high-energy impact responses of all the fiber-sizing conditions is shown in figure 7.  Representative examples of the projected damage areas on the actual samples are shown in figure 8.  The damage areas for all fiber-sizing conditions are summarized in table 2 and plotted in figure 9.

## 3.4  Composite Compression After Impact Properties

Previously reported references have stated that the impact performance and damage tolerance of glass fiber-reinforced composites are profoundly influenced by the choice of silane-coupling agent used to treat the fibers (*1*).  As impact resistance is increased by means of an incompatible silane-coupling agent, the structural performance of the composite decreases (*5*).  The decreases in structural performance and damage tolerance brought about by the use of incompatible silane coupling agents is readily evident in compression after impact (CAI) testing.  The results obtained for the compatible- and incompatible-sized fiber-reinforced composites of this study confirm such previous literature findings.  Our results show an ~45% decrease in CAI strength of

15

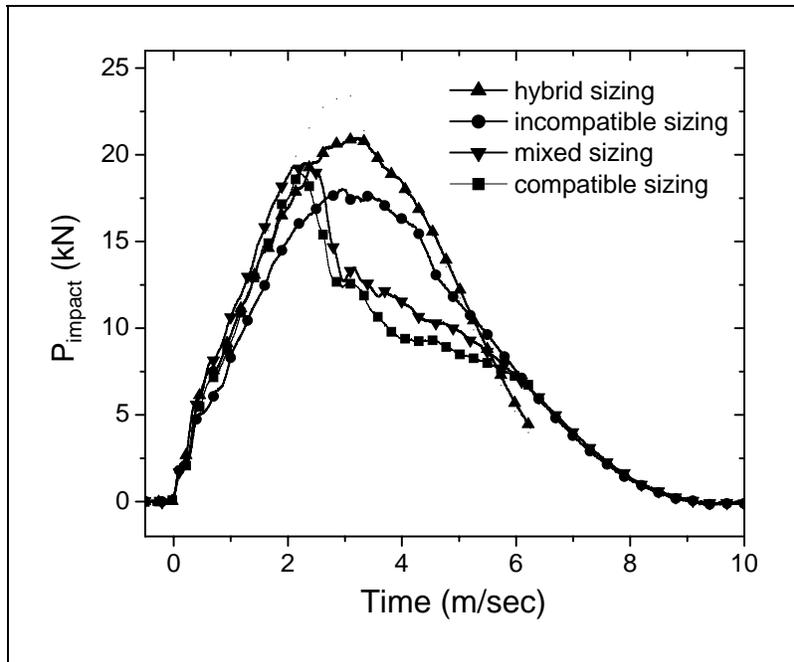Figure 7. Comparison of composite panel impact response for E-glass fibers treated with hybrid, compatible, mixed, and incompatible fiber sizings. $E_{impact}$ = 124 J, $V_{impact}$ = 4.5 m/s.
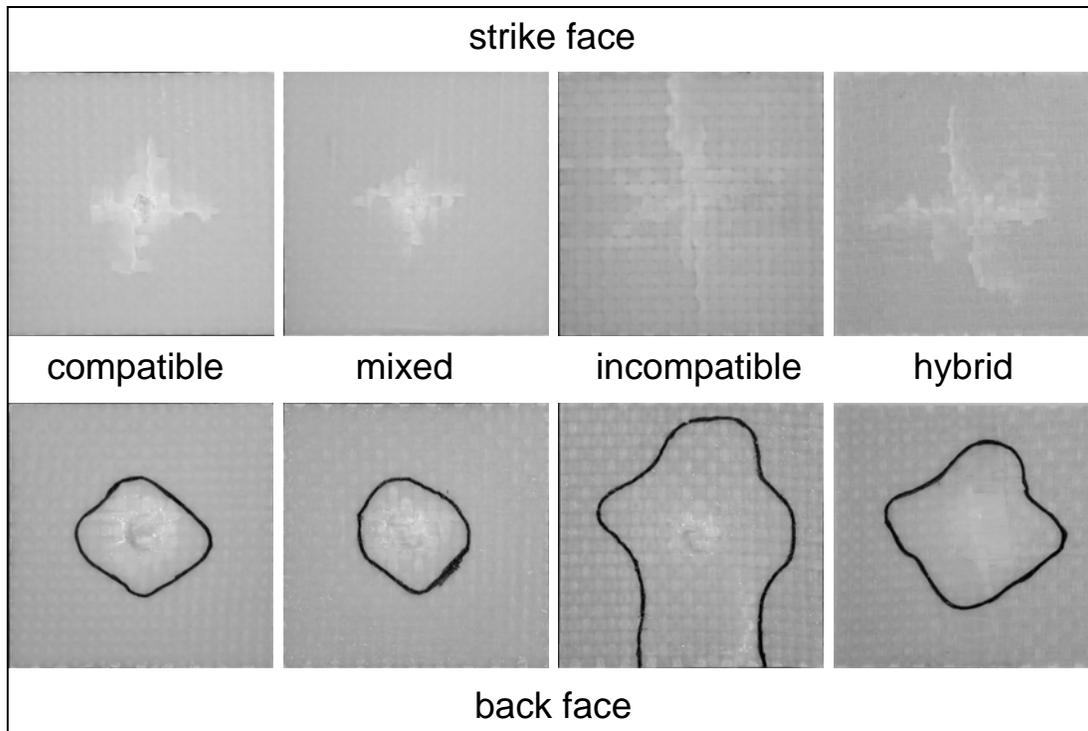


Figure 8. Images of the strike face and back face of composite panel samples after impact testing. Projected damage areas are outlined on the back faces of the samples. $E_{impact}$ = 124 J, $V_{impact}$ = 4.5 m/s.
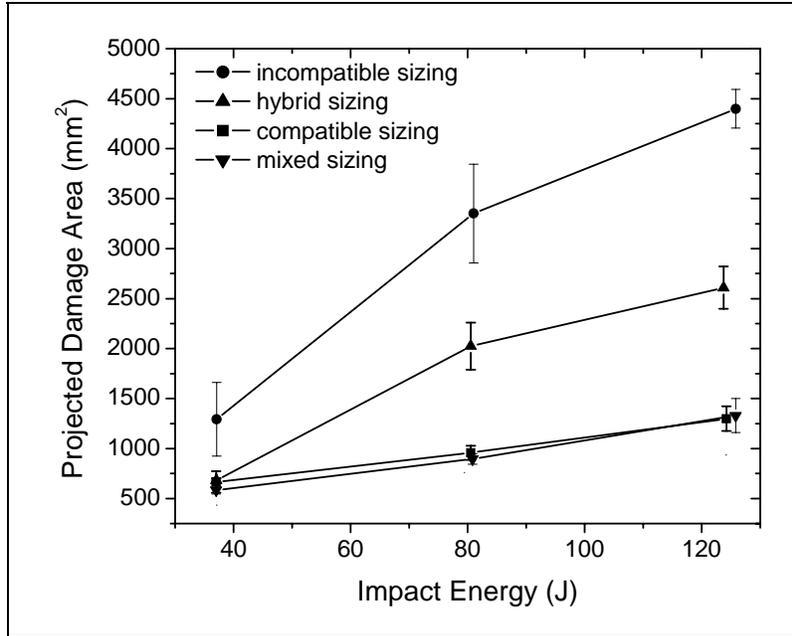
Figure 9. Damage area-vs.-impact energy plots for composite panels with
E-glass fibers treated with hybrid, compatible, mixed, and
incompatible fiber sizings. $V_{impact}$ = 4.5 m/s, straight lines drawn
between data points.

the composite from 146.0 ± 0.2 MPa to 80.5 ± 6.8 MPa when comparing the structural
compatible fiber sizing to the impact resistant incompatible sizing, respectively. The mixed
fiber-sizing treatment resulted in a slight increase in residual compressive strength at 160.6
± 2.1 MPa. The mixed fiber-sizing treatment also yielded improved impact performance in
comparison to the compatible fiber-sizing treatment. The hybrid sizing fiber treatment resulted
in a residual compressive strength of 134.4 ± 7.4 MPa, which is analogous to the compatible
sizing and notably increased from the incompatible fiber-sizing treatment. The high residual
compressive strength results for the hybrid fiber-sizing treatment are significant as this fiber-
sizing treatment provided the best drop-tower impact performance. The CAI results are
summarized in table 3.

Table 3. Summary of compression after impact testing results for composite panels with
E-glass fibers treated with hybrid, compatible, mixed, and incompatible fiber
sizings. Error represents one standard deviation.

| Fiber Sizing | $E_{impact}$ (J) | $\sigma_{ult}$ (MPa) |
|---|---|---|
| Hybrid | 42.6 ± 0.3 | 134.4 ± 7.4 |
| Compatible | 42.8 ± 0.1 | 146.0 ± 7.7 |
| Mixed | 42.5 ± 0.5 | 160.6 ± 2.1 |
| Incompatible | 42.7 ± 0.2 | 80.5 ± 6.8 |

17

## 3.5 Composite Wet Properties

As stated in the introduction section, an important function of the silane coupling agent constituent of the fiber-sizing package is to protect the glass fibers from moisture attack. If the silane coupling agent does not properly protect the glass fibers from moisture ingress, then corrosion of the glass fibers occurs, which leads to significant reductions in the mechanical performance of the composite. As a preliminary gauge of the effectiveness of the hybrid sizing to protect the glass fibers against moisture exposure, the hybrid sizing was compared directly to the compatible sizing via moisture uptake at 70 °C using small composite coupon samples. Based on previous experience with moisture uptake experiments, the compatible sizing should perform well in response to moisture attack (*54*). Poor moisture protection due to the hybrid sizing would be expected to yield significant increases in mass uptake when compared to the compatible sizing.

The moisture uptake mass percentage-vs.-time plots for composite samples reinforced with fibers treated with the compatible sizing and hybrid sizing are shown figure 10. Also illustrated in this plot is the moisture uptake curve for the neat epoxy matrix with no fiber reinforcement. All moisture uptake percentages for the composite panels have been normalized by the mass fraction of matrix contained in each sample. The neat epoxy exhibited nearly Fickian moisture uptake diffusion and began to achieve equilibration after approximately one month of exposure time (*55*). The moisture uptake curves of the composite samples deviate significantly from Fickian behavior and continue to gain mass after the neat epoxy has reached equilibrium, indicative of microcracking and voiding near the fiber-matrix interphase (*56*). After 6 months of exposure, all of the composite samples appeared discolored and physically degraded, irrespective of the fiber-sizing treatment. This is not unexpected as submersion in water at 70 °C represents a harsh environmental condition intended for rapid screening and could lead to corrosion of the glass fibers over extended periods of time, despite the use of a silane coupling agent. The important conclusion from the moisture uptake data is that the hybrid-fiber sizing does not significantly alter the moisture uptake behavior of the composite in comparison to the conventional compatible sizing.

In addition to studying the long term moisture uptake behavior of small composite coupon samples, impact and IFSS properties were also measured using the appropriate dimension samples after 30 days of moisture exposure at 70 °C. The drop tower impact results are plotted in figure 11 and summarized in table 4. The compatible and hybrid fiber-sizing treatments both yielded decreased impact properties in comparison to dry counterparts with respect to energy absorption parameters and total damage area. However, the hybrid fiber-sizing fiber treatment continues to out perform the compatible fiber sizing, as clearly seen in the force-vs.-time plots of figure 11. The short beam shear testing of the moisture exposed composite rods and subsequent calculations of IFSS yielded 41.1 ± 2.3 MPa vs. 41.1 ± 3.7 MPa for the hybrid and compatible fiber sizings, respectively. These results indicate that the moisture protection of the hybrid fiber sizing is equivalent to the moisture protection of the traditional compatible fiber sizing.
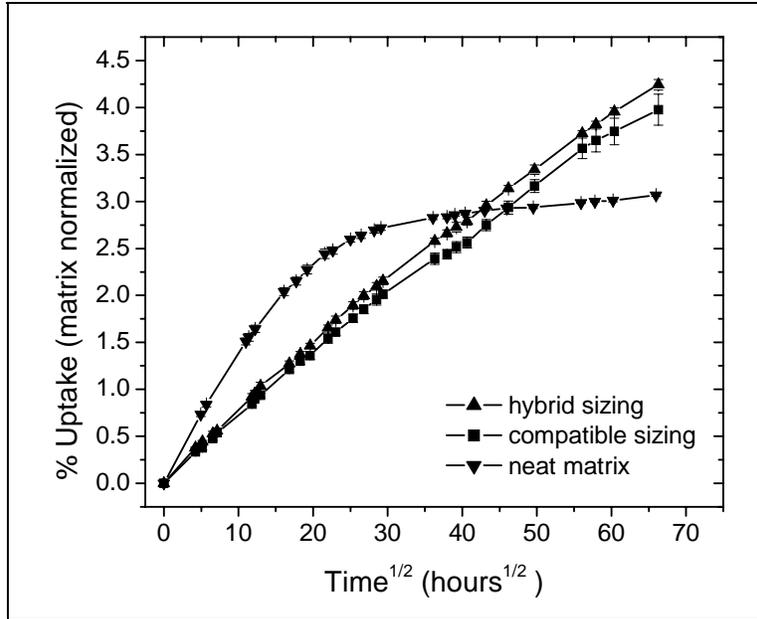
Figure 10.  Moisture uptake results for composite samples reinforced
with fibers treated with the hybrid and compatible fiber
sizings upon moisture exposure at 70 °C for ~180 days.
Moisture uptake mass percentages have been normalized to
the matrix epoxy mass fraction in each composite.  The
moisture uptake properties of the neat matrix epoxy are
shown.  Error bars represent one standard deviation.
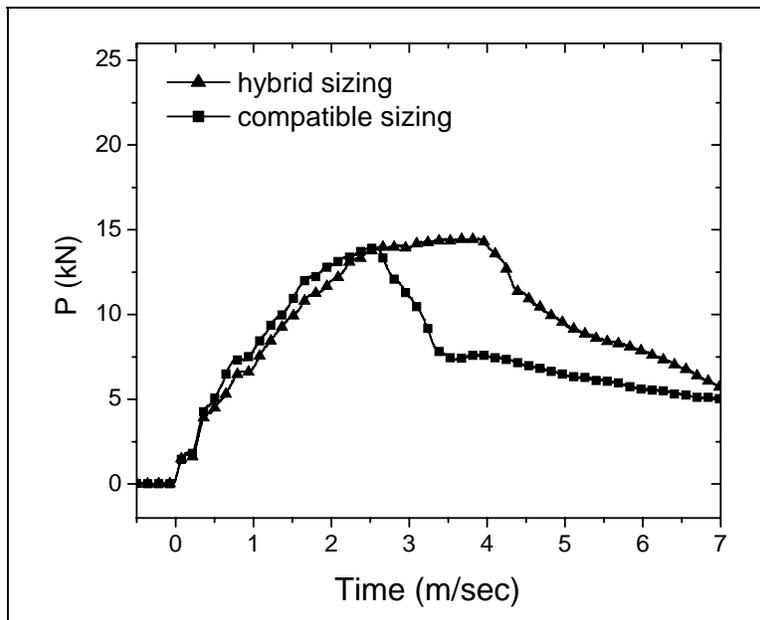


Figure 11.  Comparison of composite panel impact response for E-glass
fibers treated with hybrid and compatible sizings after
submersion in water at 70 °C for 30 days.  $E_{impact} = 124$ J,
$V_{impact} = 4.5$ m/s.

Table 4. Summary of composite panel impact response for E-glass fibers treated with hybrid and compatible sizings after submersion in water at 70 °C for 30 days. Error represents one standard deviation. $E_{impact}$ = 124 J, $V_{impact}$ = 4.5 m/s.

| Fiber Sizing | $P_{max}$ (kN) | $E_{max}$ (J) | $E_{total}$ (J) | Damage Area (mm$^2$) |
|---|---|---|---|---|
| Hybrid | 14.8 ± 0.4 | 105.5 ± 11.2 | 109.8 ± 0.8 | 3460 ± 280 |
| Compatible | 14.1 ± 0.6 | 82.5 ± 3.9 | 119.3 ± 2.1 | 1660 ± 450 |

# 4. Conclusions

The achievement of excellent structural properties with concurrent superior impact energy absorption characteristics in glass fiber-reinforced composites has traditionally been unobtainable.  The chemistry of the fiber-matrix interphase has been determined to be the key driving force in determining if optimal structural or impact properties from the composite material are to be realized, with one aspect of performance being traded for the other.  Through a careful understanding of the failure mechanisms during fiber-matrix push-out, associated energy absorption relationships, and viscoelastic properties of the fiber-matrix interphase, a novel hybrid fiber sizing was developed with the intention to provide concurrent excellent structural and impact energy absorption capability.  Furthermore, increasing the surface roughness of the fibers enhanced the impact energy absorption capabilities of the composites tested.  This new type of hybrid fiber sizing was successfully manufactured at a commercial production facility with minimal production difficulties and incurring no added cost in comparison to a standard, structural fiber sizing.  The new hybrid fiber sizing shows no significant differences when compared to the assets of a structural fiber sizing, which offers good moisture absorption protection and high CAI strengths.  The new hybrid fiber sizing also exceeds the impact performance of a traditional incompatible fiber sizing.  While the rate dependency of the hybrid fiber sizing's structural and impact response needs to be further investigated, it appears that these novel inorganic-organic hybrid fiber sizings offer the potential to achieve noncompromised structural and impact energy absorption properties simultaneously in a glass fiber-reinforced composite assembly.

# 5. References

1. Kim, J. K.; Sham, M. L.  Impact and Delamination Failure of Woven-Fabric Composites. *Composites Science and Technology* **2000**, *60*, 745–761.

2. Cantwell, W. J.; Tato, W.; Kausch, H. H.  The Influence of a Fiber-Matrix Coupling Agent on the Properties of a Glass Fiber/Polypropylene GMT. *Journal of Thermoplastic Composite Materials* **1992**, *5*, 304–317.

3. Kim, J. K.; Sham, M. L.; Sohn, M. S.; Hamada, H.  Effect of Hybrid Layers With Different Silane Coupling Agents on Impact Response of Glass Fabric Reinforced Vinylester Matrix Composites. *Polymer* **2001**, *42*, 7455–7460.

4. Peterson, B. L.; Pangborn, R. N.; Pantano, C. G.  Static and High Strain Rate Response of a Glass Fiber Reinforced Thermoplastic. *Journal of Composite Materials* **1991**, *25*, 887–906.

5. Hartman, D. R.  Ballistic Impact Behavior of High-Strength Glass-Fiber Composites. *41st Annual Conference, Reinforced Plastics/Composites Institute*, The Society of the Plastics Industry, Inc., 27–31 January 1986.

6. Kessler, A.; Bledzki, A.  Correlation Between Interphase-Relevant Tests and the Impact-Damage Resistance of Glass/Epoxy Laminates With Different Surface Treatments. *Composites Science and Technology* **2000**, *60*, 125–130.

7. Hirai, Y.; Hamada, H.; Kim, J. K.  Impact Response of Woven Glass-Fabric Composites – I. Effect of Fibre Surface Treatment. *Composites Science and Technology* **1998**, *58*, 91–104.

8. Cantwell, W. J.; Morton, J.  The Impact Resistance of Composite Materials – A Review. *Composites* **1991**, *22*, 347–362.

9. Thomason, J. L.; Dwight, D. W.  The Use of XPS for Characterization of Glass Fibre Coatings. *Composites Part A* **1999**, *30*, 1401–1413.

10. Larson, B. K.; Drzal, L. T.; Van Antwerp, J.  Swelling and Dissolution Rates of Glass Fiber Sizings in Matrix Resin Via Micro-Dielectrometry. *Polymer Composites* **1995**, *16*, 415–420.

11. Wu, H. F.; Dwight, D. W.; Huff, N. T.  Effects of Silane Coupling Agents on the Interphase and Performance of Glass-Fiber-Reinforced Polymer Composites. *Composites Science and Technology* **1997**, *57*, 975–983.

12. Ishida, H.; Koenig, J. L.  Fourier-Transform Infrared Spectroscopic Study of Structure of Silane Coupling Agent on E-Glass Fiber. *Journal of Colloid Interface Science* **1978**, *64*, 565–576.

13. Drzal, L. T.  The Role of the Fiber-Matrix Interphase on Composite Properties.  *Vacuum* **1990**, *41*, 1615–1618.

14. Fink, B. K.; McCullough, R. L.  Interphase Research Issues.  *Composites Part A* **1999**, *30,* 1–2.

15. Wang, D.; Jones, F. R.  Surface Analytical Study of the Interaction Between γ-Amino Propyl Triethoxysilane and E-Glass Surface.  *Journal of Materials Science* **1993**, *28*, 2481–2487.

16. Horner, M. R.; Boerio, F. J.; Clearfield, H. M.  An XPS Investigation of the Adsorption of Aminosilanes Onto Metal Substrates:  In *Silanes and Other Coupling Agents*; Mittal, K. L., Ed.; VSP:  Netherlands, 1992; pp 241–262.

17. Kim, J. K.; Hodzic, A.  Nanoscale Characterization of Thickness and Properties of Interphase in Polymer Matrix Composites.  *Journal of Adhesion* **2003**, *79*, 383–414.

18. Ishida, H.; Koenig, J. L.  The Reinforcement Mechanism of Fiber-Glass Reinforced Plastics Under Wet Conditions:  A Review.  *Polymer Engineering and Science* **1978**, *18*, 128–144.

19. Saidpour, S. H.; Richardson, M. O. W.  Glass Fibre Coating for Optimum Mechanical Properties of Vinyl Ester Composites.  *Composites Part A* **1997**, *28A*, 971–975.

20. Park, S. J.; Jin, J. S.  Effect of Silane Coupling Agent on Interphase and Performance of Glass Fibers/Unsaturated Polyester Composites.  *Journal of Colloid Interface Science* **2001**, *242*, 174–179.

21. Salmon, L.; Thominette, F.; Pays, M. F.; Verdu, J.  Hydrolytic Degradation of Model Networks Simulating the Interfacial Layers in Silane-Coupled Epoxy/Glass Composites. *Composites Science and Technology* **1997**, *57*, 1119–1127.

22. Gorowara, R. L.; Kosik, W. E.; McKnight, S. H.; McCullough, R. L.  Molecular Characterization of Glass Fiber Surface Coatings for Thermosetting Polymer Matrix/Glass Fiber Composites.  *Composites Part A* **2001**, 32, 323–329.

23. Tanoglu, M.; McKnight, S. H.; Palmese, G. R.; Gillespie, J. W.  A New Technique to Characterize the Fiber/Matrix Interphase Properties Under High Strain Rates.  *Composites Part A* **2000**, *31*, 1127–1138.

24. Tanoglu, M.; McKnight, S. H.; Palmese, G. R.; Gillespie, J. W.  The Effects of Glass-Fiber Sizings on the Strength and Energy Absorption of the Fiber/Matrix Interphase Under High Loading Rates.  *Composites Science and Technology* **2001**, *61*, (2), 205–220.

25. Lee, I.; Wool, R. P.  Polymer Adhesion vs. Substrate Receptor Group Density. *Macromolecules* **2000**, *33*, 2680–2687.

26. Kent, M. S.; Yim, H.; Matheson, A.; Cogdill, C.; Nelson, G.; Reedy, E. D.  Use of Self-Assembled Monolayers at Variable Coverage to Control Interface Bonding in a Model Study of Interfacial Fracture:  Pure Shear Loading.  *Journal of Adhesion* **2001**, *75*, 267–298.

27. Jensen, R. E.; McKnight, S. H.  Novel Silane Based Fiber Sizings for Enhanced Energy Absorption.  *Proceedings of the 25th Annual Meeting of the Adhesion Society and the Second World Congress on Adhesion and Related Phenomena*, Orlando, FL, February 2002.

28. Haas, K. H.; Schwab, S. A.; Rose, K.  Functionalized Coating Materials Based on Inorganic-Organic Polymers.  *Thin Solid Films* **1999**, *351*, 198–203.

29. Langroudi, A. E.; Mai, C.; Vigier, G.; Vassoille, R.  Hydrophobic Hybrid Inorganic-Organic Thin Film Prepared by Sol-Gel Process for Glass Protection and Strengthening Applications.  *Journal of Applied Polymer Science* **1997**, *65*, 2387–2393.

30. Chen, J. I.; Chareonsak, R.; Puengripat, V.; Marturunkakul, S.  Organic/Inorganic Composite Materials for Coating Applications.  *Journal of Applied Polymer Science* **1999**, *74*, 1341–1346.

31. Nikolic, L.; Radonjic, L.  Effect of the Silica Sol-Gel Coatings on the Properties of Glass Substrate.  *Ceramics International* **1998**, *24*, 547–552.

32. Choe, S.; Lin, L. S.  Effect of Colloidal Silica on Adhesion of Glass Fibres to Polypropylene.  *Polymers & Polymer Composites* **2001**, *9*, 175–183.

33. Thomason, J. L.  The Interface Region in Glass Fibre-Reinforced Epoxy Resin Composites:  3.  Characterization of Fibre Surface Coatings and Interphase.  *Composites* **1995**, *26*, 487–498.

34. ASTM D 3379-75, Standard Test Method for Tensile Strength and Young's Modulus for High-Modulus Single-Filament Materials.  *Annu. Book ASTM Stand.*, 1975.

35. Thomason, J. L.  The Interface Region in Glass Fibre-Reinforced Epoxy Resin Composites:  1.  Sample Preparation, Void Content and Interfacial Strength.  *Composites* **1995**, *26*, 467–475.

36. Gorowara, R. L.  *Interphase Formation and Environmental Degradation in Glass Fiber/Vinyl Ester Composites*; technical report; Center for Composite Materials:  University of Delaware, 2001–2002, p 97.

37. Hsiao, K. T.; Gillespie, J. W.; Advani, S. G.; Fink, B. K.  Role of Vacuum Pressure and Port Locations on Flow Front Control for Liquid Composite Molding Processes.  *Polymer Composites* **2001**, *22*, 660–667.

38. ASTM D 792-00. Standard Test Methods for Density and Specific Gravity (Relative Density) of Plastics by Displacement. *Annu. Book ASTM Stand.*, 2001.

39. ASTM D 4475-85. Standard Test Method for Apparent Horizontal Shear Strength of Pultruded Reinforced Plastic Rods by the Short-Beam Method. *Annu. Book ASTM Stand.*, 1985.

40. ASTM D 790-96a. Standard Test Methods for Flexural Properties of Unreinforced and Reinforced Plastics and Electrical Insulating Materials. *Annu. Book ASTM Stand.*, 1997.

41. ASTM D 3039 and D 3039M-95a. Standard Test Methods for Tensile Properties of Polymer Matrix Composite Materials. *Annu. Book ASTM Stand.*, 1995.

42. Instron Dynatup 930-1, version 1.21.

43. Rasband, W. *ImageJ version 1.30*. National Institute of Health.

44. Suppliers of Advance Composite Materials Association, SACMA Recommended Test Method for Compression After Impact Properties of Oriented Fiber-Resin Composites. SRM 2R-94; SACMA, 1994.

45. Brown, E. N.; Davis, A. K.; Jonnalagadda, K. D.; Sottos, N. R. Effect of Surface Treatment on the Hydrolytic Stability of E-Glass Fiber Bundle Strength. *Composites Science and Technology* **2005**, *65*, 129–136.

46. Ikuta, N.; Maekawa, Z.; Hamada, H.; Ichihashi, M.; Nishio, E. Evaluation of Interfacial properties in Glass Fibre-Epoxy Resin Composites--Reconsideration of an Embedded Single Filament Shear-Strength Test. *Journal of Materials Science* **1991**, *26*, 4663–4666.

47. Cheeseman, B. A.; Bogetti, T. A. Ballistic Impact into Fabric and Compliant Laminates. *Composite Structures* **2003**, *61*, 161–173.

48. Dear, J. P.; Brown, S. A. Impact Damage Processes in Reinforced Polymeric Materials. *Composites Part A* **2003**, *34*, 411–420.

49. Hosur, M. V.; Karim, M. R.; Jeelani, S. Experimental Investigations on the Response of Stitched/Unstitched Woven S2-Glass/SC15 Epoxy Composites Under Single and Repeated Low Velocity Impact Loading. *Composite Structures* **2003**, *61*, 89–102.

50. Ruhala, L. A.; Engel, R. S. An Investigation of Fiber Volume Fraction on the Impact Properties of Fiber Reinforced Composite Laminate Plates. *Journal of Reinforced Plastics and Composites* **2000**, *19*, 449–464.

51. Rydin, R. W.; Karbhari, V. M.  Partitioning Energy During Low-Velocity Impact of RTM Fiber-Reinforced Composites. *International Journal of Impact Engineering* **1998**, *21*, 773–789.

52. Karbhari, V. M.  Impact Characterization of RTM Composites. *Journal of Materials Science* **1997**, *32*, 4159–4166.

53. Lee, D. G.; Lim, T. S.; Cheon, S. S.  Impact Energy Absorption Characteristics of Composite Structures. *Composite Structures* **2000**, *50*, 381–390.

54. Jensen, R. E.; Johnson, C. E.; Ward, T. C.  Investigation of a Waterborne Epoxy for E-Glass Composites. *Journal of Polymer Science:  Part B: Polymer Physics* **2000**, *38*, 2351–2365.

55. Chen, C. H.; Springer, G. S.  Moisture Absorption and Desorption of Composite Materials. *Journal of Composite Materials* **1976**, *10*, 2–20.

56. Wang, J. Y.; Ploehn, H. J.  Dynamic Mechanical Analysis of the Effect of Water on Glass Bead Epoxy Composites. *Journal of Applied Polymer Science* **1996**, *59*, 345–357.

NO. OF
COPIES  ORGANIZATION

    1       DEFENSE TECHNICAL
  (PDF     INFORMATION CTR
 ONLY)    DTIC OCA
          8725 JOHN J KINGMAN RD
          STE 0944
          FORT BELVOIR VA 22060-6218

    1       US ARMY RSRCH DEV &
            ENGRG CMD
            SYSTEMS OF SYSTEMS
            INTEGRATION
            AMSRD SS T
            6000 6TH ST STE 100
            FORT BELVOIR VA  22060-5608

    1       INST FOR ADVNCD TCHNLGY
            THE UNIV OF TEXAS
            AT AUSTIN
            3925 W BRAKER LN
            AUSTIN TX 78759-5316

    1       DIRECTOR
            US ARMY RESEARCH LAB
            IMNE ALC IMS
            2800 POWDER MILL RD
            ADELPHI MD 20783-1197

    3       DIRECTOR
            US ARMY RESEARCH LAB
            AMSRD ARL CI OK TL
            2800 POWDER MILL RD
            ADELPHI MD 20783-1197

    3       DIRECTOR
            US ARMY RESEARCH LAB
            AMSRD ARL CS IS T
            2800 POWDER MILL RD
            ADELPHI MD 20783-1197


            ABERDEEN PROVING GROUND

    1       DIR USARL
            AMSRD ARL CI OK TP (BLDG 4600)

INTENTIONALLY LEFT BLANK.